#6165

Ventilation by Displacement: Calculation of the Flow in Vertical Plumes

V. Shankar, L. Davidson, E. Olsson
Dept. of Thermo and Fluid Dynamics
Chalmers University of Technology
S-412 96 Gothenburg, Sweden

Summary

In displacement ventilation systems air is supplied to the room at low velocity at a volume flow rate $\dot{V}_{in}$. The temperature of the supplied air is slightly lower than that of the room. Air is heated by the objects in the room (e.g., persons, photo copy machines, etc.) and it rises due to buoyancy. The rising flow above the heat sources resembles a plume.

The flow in the plumes rises upto the ceiling. The volume flow rate in plumes for a given vertical distance from the heat source x, is $\dot{V}_{plume}(x)$ and increases with x. At the ceiling the flow spreads out laterally. Air is extracted below the celing at a rate of $\dot{V}_{in}$. The remaining of the flow, $\dot{V}_{plume}(H) - \dot{V}_{in}$ (H is the height of the room) flows downwards. The level x_{front}, where this downward flow has all been entrained in the plumes occurs when $\dot{V}_{in} = \dot{V}_{plume}$.

From the discussion above it is clear that knowledge of the volume flow rate in plume is crucial for the efficient performance of the displacement ventilation system.

Investigations have been carried out simulating the flow in a complete room. Here an elliptic solver was used [1]. In this approach the flow in the plume is not accurately resolved due to limitations in grid resolutions.

The aim of the present investigation is to study the flow in verticle plumes. The nature of flow in these configurations is parabolic in the flow direction (see Fig.1). This means that the flow at a given vertical level (plane i) is not influenced by the flow conditions at plane $i+1$. This allows us to use a forward marching technique, i.e., a parabolic solver in vertical direction. A solver of this type is extremly fast when compared to an elliptic solver (up to 100 times faster). This allows us to prosecute parameter studies, and to ensure that the solutions are grid independent.

It was found that the standard $k-\varepsilon$ model does not predict spreading rates in agreement with experimental data. Therefore two modifications of the model were introduced.

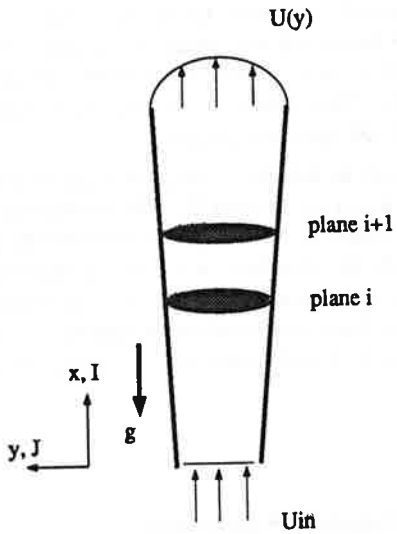

Figure 1: *Vertical plume*

1 Introduction

1.1 Background

Since displacement flow systems has become increasingly popular and is replacing the traditional mixing flow systems, it is of great interest to prosecute numerical investigation of the flow. In displacement flow system air is supplied at low velocity through a large inlet device near the floor. The temperature of the supply air is lower than the room's temperature. In order to design a displacement ventilation system which can synchronize with the comfort ventilation in rooms. It is therefore important to predict the nature of flow over a heat source.

At the department we have carried out calculations of the flow in rooms ventilated by displacement technique [1]. The experience was that the computer times was prohibitively large, due to the strong coupling of the temperature and the vertical momentum equation. For calculations of this type it means that either

i) the CPU time is so high that no parameter studies can be done, or

ii) one can not afford to use sufficiently fine grids.

1.2 Aim

The object of present investigation is to study the flow in vertical plumes, which in rooms ventilated with displacement ventilation, are formed above the heat sources (e.g. persons, terminals, photo copy machines). The nature of flows in these configurations is parabolic in the flow direction (see Fig. 1), i.e., that the flow at a given

vertical level (plane i) is not influenced by the flow conditions at plane $i+1$. This allows us to use a space marching technique, i.e. a parabolic solver in the vertical direction. A solver of this type is extremly fast when compared to an elliptic solver (up to 100 times faster). This allows us to prosecute parameter studies, and to ensure that the solutions are grid independent.

This paper is presented as follows. The governing equations for mean flow and turbulent quantites are given in Section 2. The numerical code used is described in Section 3. Section 4 deals with the special features of parabolic flows. It was found necessary to modify the standard $k-\varepsilon$ turbulence model in order to obtain the spreading rate of plane plume in agreement with experiments. This modification is given in Section 5. The boundary conditions and results are presented in Section 6 and Section 7 respectively. Conclusions are drawn in the last section.

2 Equations

2.1 General Transport Equation

The general transport equation in Cartesian coordinates for a variable Φ is

$$\frac{\partial}{\partial x_m}(\rho U_m \Phi) = \frac{\partial}{\partial x_m}\left(\Gamma_\Phi \frac{\partial \Phi}{\partial x_m}\right) + \overline{S}^\Phi, \tag{1}$$

where $\overline{S}^\Phi$ denotes the source per unit volume for the variable Φ. The flux vector J_m, containing convection and diffusion terms are defined as follows

$$J_m = \rho U_m \Phi - \Gamma_\Phi \frac{\partial \Phi}{\partial x_m}. \tag{2}$$

Substituting Eq. (2) into Eq. (1), we get

$$\frac{\partial J_m}{\partial x_m} = \overline{S}^\Phi.$$

Or in vector notation, we have

$$\nabla \cdot \mathbf{J} = \overline{S}^\Phi.$$

Integrating the above equation over a typical control volume with volume V and surface area A, and using the Gauss' law we get

$$\int_A \mathbf{J} \cdot \mathbf{dA} = \int_V \overline{S}^\Phi dV. \tag{3}$$

2.2 Mean Flow Equations

We have the continuity equation

$$\frac{\partial}{\partial x_i}(\rho U_i) = 0. \tag{4}$$

The momentum equation is expressed as

$$\frac{\partial}{\partial x_j}(\rho U_i U_j) = -\frac{\partial p}{\partial x_i} + \frac{\partial}{\partial x_j}\left(\mu_{eff}\frac{\partial U_i}{\partial x_j}\right) + \rho_{ref} g_i \frac{T - T_{ref}}{T_{ref}}, \tag{5}$$

where $g_1 = 0$, $g_2 = -g$, and where the Boussineq approximation is used for the gravitation term.

The governing equation for temperature is given by

$$\frac{\partial}{\partial x_j}(\rho U_i T) = \frac{\partial}{\partial x_j}\left(\frac{\mu_{eff}}{\sigma_t}\frac{\partial T}{\partial x_j}\right), \tag{6}$$

where the turbulent Prandlt number $\sigma_t = 0.7$.

2.3 Turbulence Model

The standard $k - \varepsilon$ turbulence model is used. The transport equations for k and ε can be written in tensor notation as

$$\frac{\partial}{\partial x_j}(\rho U_j k) = \frac{\partial}{\partial x_j}\left(\frac{\mu_{eff}}{\sigma_k}\frac{\partial k}{\partial x_j}\right) + P_k + G_B - \rho\varepsilon \tag{7}$$

$$\frac{\partial}{\partial x_j}(\rho U_j \varepsilon) = \frac{\partial}{\partial x_j}\left(\frac{\mu_{eff}}{\sigma_\varepsilon}\frac{\partial \varepsilon}{\partial x_j}\right) + c_{\varepsilon 1}\frac{\varepsilon}{k}(P_k + G_B - c_{\varepsilon 2}\rho\varepsilon). \tag{8}$$

where $c_\varepsilon 1 = 1.92, c_\varepsilon 2 = 1.44, \sigma_k = 1.0$ and $\sigma_\varepsilon = 1.3$. Since the Boussineq approximation is used, the density in Eqns. 4-8 is constant.

The generation term P_k can be expressed in tensor notation as

$$P_k = \mu_t \frac{\partial U_i}{\partial x_j}\left(\frac{\partial U_i}{\partial x_j} + \frac{\partial U_j}{\partial x_i}\right), \tag{9}$$

and the production due to buoyancy can be written as

$$G_B = \rho g \frac{\overline{u\theta}}{T_{ref}}, \tag{10}$$

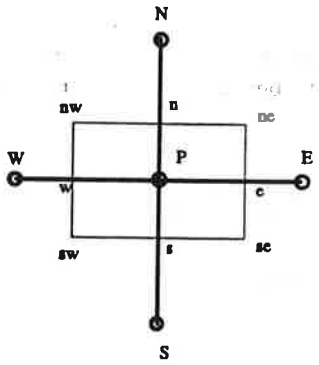

Figure 2: *Control volume and notation (for clarity Fig. 2 is drawn in Cartesian coordinate system).*

where

$$\rho\overline{u\theta} = -\frac{\mu_t}{\sigma_t}\frac{\partial T}{\partial x}. \tag{11}$$

The turbulent viscosity μ_t is calculated as

$$\mu_t = \rho c_\mu \frac{k^2}{\varepsilon}.$$

The effective viscosity μ_{eff} is obtained as

$$\mu_{\text{eff}} = \mu + \mu_t.$$

3 The Code

3.1 Basis

In this section the parabolic version of CALC-BFC, developed by Farhanieh and Davidson [2], is presented. This is a derivative of the standard three-dimensional finite volume computer program CALC-BFC [3] (Boundary Fitted Coordinates) for three-dimensional complex geometries. The program uses Cartesian velocity components, and the pressure-velocity coupling is handled with the SIMPLEC procedure. In most finite volume programs staggered grids for the velocities have been used [4]. In the present work collocated variables are used, which means that velocities are stored along with all scalar variables like p, k, ε at the centre of the contol volume. This concept was suggested by Rhie and Chow [5].

Equation 3 is discretized using standard control volume formulation as described by Patankar [4]. Integrating Eq. 3 over a control volume (See Fig 2) yields

$$(\mathbf{J}\cdot\mathbf{A})_e + (\mathbf{J}\cdot\mathbf{A})_w + (\mathbf{J}\cdot\mathbf{A})_n + (\mathbf{J}\cdot\mathbf{A})_s + (\mathbf{J}\cdot\mathbf{A})_h + (\mathbf{J}\cdot\mathbf{A})_l = S^\Phi \delta V.$$

Note that the positive signs on the terms containing contributions from west and south surfaces will be negative because the scalar products in themselves are negative.

The discretized equation will be of the form

$$a_P \Phi_P = \sum_n b a_{nb} \Phi_{nb} + S_C^\Phi, \tag{12}$$

where

$$a_P = \sum a_{nb} - S_P^\Phi.$$

The coefficients a_{nb} contain the contributions due to both convection and diffusion. The source terms S_C^Φ and S_P^Φ contain the remaining terms.

3.2 Convection

The convection which is the first part of the flux vector **J** (Eq. 2), is the scalar product of the velocity vector and the area vector multiplied by the density. For north face we obtain (see Fig. 3)

$$\dot{m}_n = (\rho \mathbf{u} \cdot \mathbf{A})_n = \rho_n \left(U_n A_{nx} + V_n A_{ny} + W_n A_{nz}\right).$$

Since the Cartesian areas A_{nx}, A_{ny}, A_{nz} are stored in the program, the calculation of the convective contributions to **J** is straight-forward. Special care must however be taken when the velocities are interpolated from their storage location at the cell center to the control volume faces to avoid non physical oscillations. Rhie and Chow [5] solved this problem [3].

3.3 Diffusion

Diffusion is the second part of the flux vector **J** in Eq. 2, and it has the form

$$\mathcal{D} = (\mathbf{J} \cdot \mathbf{A})_{diff} = -\Gamma_\Phi \mathbf{A} \cdot \nabla \Phi.$$

For example, the Cartesian coordinates (x, y, z) for the north face are given by,

$$-\{\Gamma_\Phi \mathbf{A} \cdot \nabla \Phi\}_n = -\left\{\Gamma_\Phi \left(A_x \frac{\partial \Phi}{\partial x} + A_y \frac{\partial \Phi}{\partial y} + A_z \frac{\partial \Phi}{\partial z}\right)\right\}_n,$$

and in curvilinear coordinates (ξ, η, ζ)

$$-\{\mathbf{A} \cdot \nabla \Phi\}_n = -\left\{\mathbf{A} \cdot \mathbf{g}_i g^{ij} \frac{\partial \Phi}{\partial \xi_j}\right\}_n = -\left\{|\mathbf{A}| \mathbf{n} \cdot \mathbf{g}_i g^{ij} \frac{\partial \Phi}{\xi_j}\right\}_n.$$

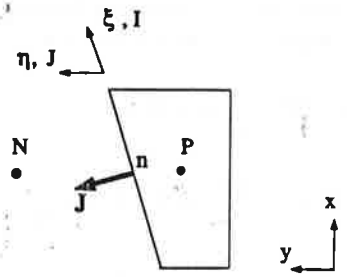

Figure 3: *The flux through the north face of a non-orthogonal control volume. ξ is along the I-grid lines, and η is along the J-grid lines.*

The covariant (tangential) base vectors $\mathbf{g}_1, \mathbf{g}_2$ and $\mathbf{g}_3$ correspond to I, J and K grid lines respectively. The metric tensor is involved because the components of the product $\mathbf{A} \cdot \mathbf{g}_i$ and the derivative $\partial\Phi/\partial\xi_j$ are both covariant, and the product of their (contravariant) base vectors is not equal to zero or one (as in Cartesian coordinate systems) since they are non-orthogonal to each other.

The diffusive terms are discretized using central differencing, which is of second order accuracy [4].

4 The Implications of Parabolic Flow

In parabolic finite volume methods, two basic assumptions are made [6]. First, the streamwise diffusion term

$$\frac{\partial}{\partial \xi}\left(\Gamma_\Phi \frac{\partial \Phi}{\partial \xi}\right),$$

is set to zero in all equations. Secondly the streamwise pressure gradient $\partial p/\partial \xi$ is set to zero.

It should be noted that in the literature, terms in the production term P_k involving $\partial/\partial\xi$-derviate are usually neglected [9, 10, 11]. Further more, some approxiamtions are also made when calculating the non-orthogonal diffusion term [11]. No such simplifications are used in the present parabolic solver.

In parabolic flow, the flow downstream (plane $i+1$, see Fig. 1) does not influence the flow upstream (plane i). This feature means that a space marching technique can be used, where the flow in each i-plane is calculated separately and only *once*. First, the flow is solved at i-plane $i = 2$ (the inlet boundary conditions are set at $i = 1$) and a convergent solution is obtained for this plane, then the flow at plane $i = 3$ is calculated, and so on. The parabolic solver is up to two orders of magnitude faster than a standard elliptic SIMPLE solver, because in an elliptic solver the flow at each i-plane is not calculated *once*, but several *hundred times*.

5 Modification of the Standard $k-\varepsilon$ Turbulence Model

5.1 The Bouyancy Production Term (Plane Plume)

It was found that the standard $k-\varepsilon$ model underestimates the spreading rate $\partial\delta_{1/2}/\partial x$ of plane plumes ($\delta_{1/2}$ denotes half-width of the plume). The standard production term due to buoyancy G_B in Eqns. 10-11 is almost negligible, because the streamwise temperature gradient is very small. In plumes, this term is positive ($\partial T/\partial x < 0$), and it should thus increase the spreading rate In order to enhance the importance of G_B and thereby increasing the spreading rate, a modification of the production term G_B, used by Ince and Launder [12] and Davidson [13] is introduced. The idea is borrowed from the general gradient hypothesis of Daly and Harlow [14] where

$$\overline{u\theta} = -c_\theta \frac{k}{\varepsilon}\left(\overline{u^2}\frac{\partial T}{\partial x} + \overline{uv}\frac{\partial T}{\partial y}\right) \tag{13}$$

and

$$c_\theta = c_{\theta 1}\frac{c_\mu}{\sigma_t}.$$

Using Boussinesq assumption for $\overline{uv}$ in the second term in Eq. 13, and substituting Eq. 11 in the first part of Eq. 13, we obtain

$$\overline{u\theta} = -\frac{\mu_t}{\rho\sigma_t}\frac{\partial T}{\partial x} + c_\theta \frac{\mu_t}{\rho}\frac{k}{\varepsilon}\frac{\partial T}{\partial y}\frac{\partial U}{\partial y}. \tag{14}$$

In [12] and [13] the constant $c_{\theta 1}$ was taken as $\frac{3}{2}$; in the present study $c_{\theta 1} = 1.7$ was found to give the best agreement with experimental data.

In Eq. 14 not only the streamwise temperature gradient $\partial T/\partial x$ is present, but also the transversal gradient $\partial T/\partial y$, which is an order of magnitude larger than $\partial T/\partial x$ is considered. In a plume both $\partial T/\partial y$ and $\overline{uv}$ are negative. Hence the prescribed modification will increase G_B which will thus enhance the buoyant production of turbulence and increases the spreading rate.

5.2 Normal Stress Amplification (NSA) [Axisymmetric Plume]

Hanjalic and Launder [15] developed a modification of the $k-\varepsilon$ model, where the the production term in the dissipation equation was made more sensitive to the irrotational strains $\partial U/\partial x, \partial V/\partial y$ in order to increase ε in axisymmetric flow and thereby reducing the spreading rate. Malin [16] has recently proposed some minor alterations in Hanjalic and Launder's model.

The modified production term in the k and ε-equation can be written [15] as

$$P_k = -\overline{uv}\frac{\partial U}{\partial y} - \left(\overline{u^2} - \overline{v^2}\right)\frac{\partial U}{\partial x}$$

	$d\delta_{1/2}/dx$
standard $k-\varepsilon$	0.068
modified $k-\varepsilon$	0.12
RSM [17]	0.079
Experiments [18]	0.12

Table 1: *Spreading rate for the plane plume.*

and

$$P_\varepsilon = -\frac{\varepsilon}{k}\left\{c_{\varepsilon 1}\overline{uv}\frac{\partial U}{\partial y} + c_{\varepsilon 3}\left(\overline{u^2}-\overline{v^2}\right)\frac{\partial U}{\partial x}\right\},$$

where the shear stress $\overline{uv}$ is taken from Boussinesq approximation, $c_{\varepsilon 3} = 4.44$ [16] and

$$\left(\overline{u^2}-\overline{v^2}\right) = c_k k$$

where $c_k = 0.39$ was choosen in order to obtain predicted spreading rate in agreement with experiments. The coefficient in the diffusion term in the ε-equation was taken as $\sigma_\varepsilon = 1.1$ [16].

6 Boundary Conditions

Inlet

All variables are prescribed according to experiments. The inlet is covered by half of the total number of nodes in the J-direction.

Symmetry line

V is set to zero, and zero gradient $\partial\Phi/\partial y$ is set for the remaining variables.

Free Boundary

The mass flux across the boundary is calculated from local continuity, and the variables are given by their free-stream values.

7 Results

The flow in plane and axi-symmetric plumes is calculated. 60 nodes are used in the transversal (J) direction, and 40-60 steps in the streamwise direction were used. The size of the forward steps was varied between 15 % and 30 % of the local width of the plume. The CPU time for one computation was about 1 minute on a DEC-3100 workstation (approximately as fast as a SUN Sparc 1+).

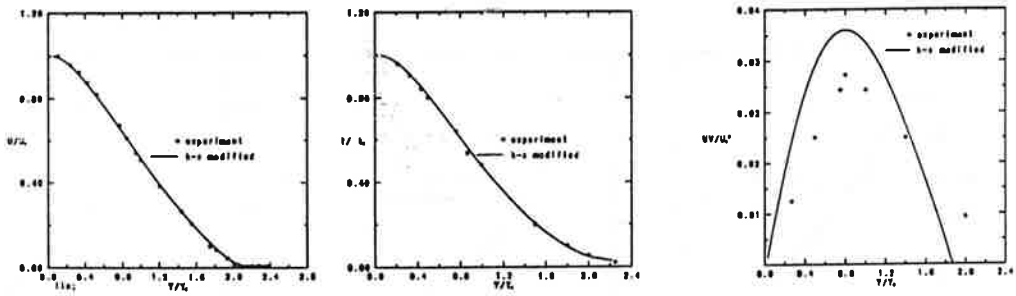

Figure 4: *Plane plume. Predicted U, T and $\overline{uv}$-profiles compared with experiments of Chandrasekhara (1989). The modification of $k-\varepsilon$ as presented in Section 5.1.*

Our code is written for three-dimensional parabolic flows. In this investigation we have calculated for two-dimensional plumes. The boundary condition for V at the symmetry line is $V = 0$, i.e., we do not need to solve the V-momentum equation or the pressure correction equation, since V can be obtained from continuity. The equation that we solve are U, T, k and ε-equations.

7.1 Plane Plume

The inlet boundary conditions $U_{in} = 0.076$ m/s , $T_{in} = 3.68$ °C and $T_a = 0$ (a denotes ambient) were used for the mean flow variables, inlet height $D = 0.01$ m, and k and ε were estimated from mixing length theory as $k_{in} = (0.01U_{in})^2$, $\varepsilon = k_{in}^{\frac{3}{2}}/0.1h$, where $h = 0.02$ m is the height of the inlet. In the stagnant surroundings all variables were set to zero. The Archimedes number is calculated as

$$Ar = \frac{gD\Delta T}{T_a U_{in}^2} = 0.23.$$

We started to use the standard $k-\varepsilon$ model, but this gave too small a spreading rate compared with experiments (see Table 1). Note that not even a full Reynolds Stress Model gives a spreading rate according to experiments (see Table 1). With the proposed modification of the heat flux $\overline{u\theta}$ in Section 5.1 we increased the predicted spreading rate to agree with experiment.

In Fig. 4 the predicted U, T and $\overline{uv}$-profiles are compared with experiments and the agreement is good.

7.2 Axi-symmetric Plume

The boundary conditions were the same as the plane plume. The NSA-modification was used. The predicted spreading rates are compared with experimental data in Table 2, and the modified $k-\varepsilon$ model gives a spreading rate in agreement with experiment, which is further confirmed from Fig. 5.

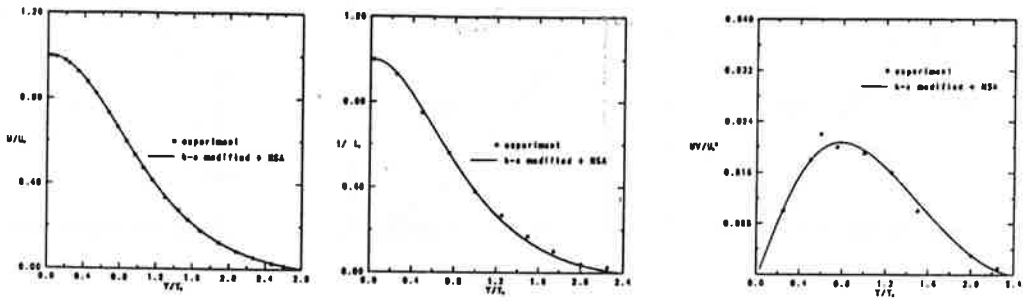

Figure 5: *Axi-symmetric plume. Predicted $U/U_c, T/T_c$ and $\overline{uv}/U_c^2$-profiles compared with experiments of Chandrasekhara (1983). The modification of $k-\varepsilon$ as presented in Section 5.2.*

	$d\delta_{1/2}/dx$
standard $k-\varepsilon$	0.10
$k-\varepsilon$ with NSA	0.12
RSM [17]	0.096
Experiments [20]	0.12

Table 2: *Spreading rate for the axi-symmetric plume.*

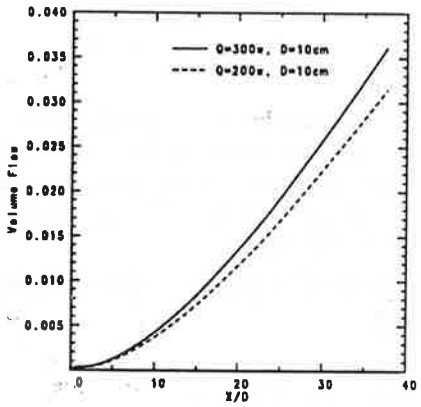

Figure 6: *Axi-symmetric plume. Volume flow rate in ax axi-symmetric plume with inlet diameter $D = 10$ cm for different heat sources. $Q = 100, 200$ and 300 W.*

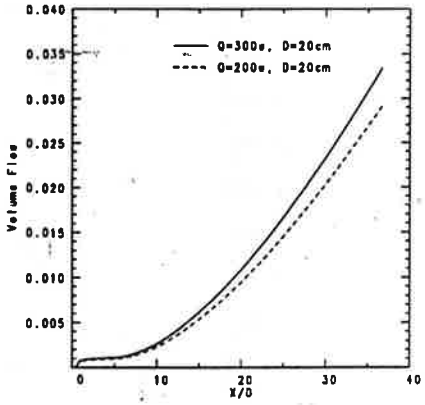

Figure 7: *Axi-symmetric plume. Volume flow rate in ax axi-symmetric plume with inlet diameter $D = 20$ cm for different heat sources. $Q = 100, 200$ and 300 W.*

7.3 Pure Axi-symmetric Plume

In the previous sections we have studied plumes with some initial momentum, i.e., inlet velocity different from zero. In this subsection we will study pure axi-symmetric plumes in stagnant surroundings. The boundary conditions at the inlet are $U_{in} = 0, T_{in} = T_a$ (subscript a denotes ambient) and a heat source Q is prescribed for temperature equations (acually Q/c_p, since we not solving for enthalpy but for temperature). This gives an Archimedes number $Ar = 0$. The traditional Grashof number

$$Gr = \frac{g\Delta T D^3}{\rho_{in}\nu_{in}^2},$$

is not defined since we do not have any temperature difference ΔT driving the plume. However, an alternative Grashof number can be defined as [20]

$$Gr_Q = \frac{gQD^2}{c_p T_a \rho_{in} \nu_{in}^3}.$$

The parameter for plume flow which a ventilation engineer is interested in is the volume flow rate $\dot{V}(x)$ in the plume as a function of the vertical height x (see Summary). In Figs. 6-8, the volume flow rate are presented for different inlet diameters D and heat sources Q. It can be seen that $\dot{V}(x)$ increases with x and Q as expected. But an increase in Q with a factor two, does not give rise to a large increase in $\dot{V}$ as indicated in Figs. 6-8. The reason for the same can be explained as follows. A fully developed turbulent plume is characterized by its initial weight deficit W_{in} [20]

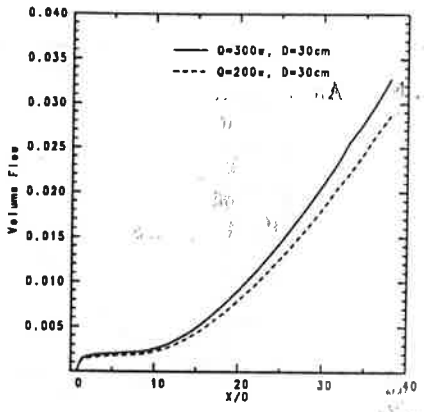

Figure 8: *Axi-symmetric plume. Volume flow rate in ax axi-symmetric plume with inlet diameter $D = 30$ cm for different heat sources. $Q = 100, 200$ and 300 W.*

$$W_{in} = \frac{gQ}{c_p T_a}, \tag{15}$$

and from dimensional analysis the characteristic velocity can be written as

$$U_c \propto \frac{W_{in}}{\rho_{in}}. \tag{16}$$

As the volume flow rate in the plume can be estimated as

$$\dot{V} \propto U_c y_{1/2}^2, \tag{17}$$

it can be seen from Eqns. 15-17 that an increase in Q with a factor of two only increases the volume flow rate with a factor $2^{\frac{1}{3}}$.

Comparing Figs. 6-8, we find that the volume flow rate $\dot{V}(x)$ does not increase as the diameter D is increased (as expected?), but rather the opposite. The spreading rate for a fully developed axi-symmetric plume is related to x as

$$y_{1/2} \propto x. \tag{18}$$

From Eqns. 16 - 18 we see that the $\dot{V}(x)$ in a fully develped plume is independent of its initial diameter D. The predicted volume flow rates in Figs. 6-8 decrease with D because the predicted length of the transition region increases with D. For $D = 10$ cm in Fig. 6 transition is predicted at $x/D \simeq 3$, whereas for $D = 30$ cm in Fig. 8 the transition does not occur until $x/D \simeq 10$.

8 Conclusions

In ventilation displacements systems plumes are formed above objects which heat the cool supplied air. The volume flow rate in the plumes is crucial for the performance of the ventilation system, and it is thus a parameter of great interest

to a ventilation engineer. While computing displacement ventilation flows, elliptic solvers have traditionally been used, an approach which is inaccurate due to poor grid resolution.

In the present work a parabolic solver has been used for computing the turbulent flow in plane and axi-symmetric plumes. In this approach a space marching technique is utilized which is upto 100 times faster than elliptic solvers. Sufficiently fine grid can thus be afforded, and parametrical studies can be prosecuted.

The standard $k-\varepsilon$ has been modified in order to give spreading rates of the plumes in agreement with experimental data. The flows in plane and axi-symmetric plumes with small inlet velocity were simulated, and good agreement with experiments was obtained. Also pure axi-symmetric plumes were studied. The inlet diameter ($D = 10, 20$ and 30 cm) and the strength of the heat source ($Q = 100, 200$ and 300 W) were varied.

References

[1] L. DAVIDSON, Ventilation by displacement in a three-dimensional room – a numerical study, *Bldg Environ* **24**, 363-392, 1989.

[2] B. FARHANIEH and L. DAVIDSON, A finite-volume code employing collocated variable arrangement and Rhie-Chow interpolation method for computation of three-dimensional parabolic flow in non-orthogonal coordinates, Rept. 92/5, Dept. of Applied Thermodynamics and Fluid Mechanics, Chalmers University of Technology, Gothenburg, Sweden, 1992.

[3] L. DAVIDSON and B. FARHANIEH, CALC-BFC: A finite-volume code employing collocated variable arrangement and Cartesian velocity components for computation of fluid flow and heat transfer in complex three-dimensional geometries, Rept., Dept. of Applied Thermodynamics and Fluid Mechanics, Chalmers University of Technology, Gothenburg, Sweden, 1991.

[4] S.V. PATANKAR, Numerical heat transfer and fluid flow, McGraw-Hill, Washington, 1980.

[5] C.M. RHIE and W.L.CHOW, Numerical study of the turbulent flow past an airfoil with trailing edge separation, *AIAA J.*, **21**, pp. 1527-1532, 1984.

[6] S.V. PATANKAR and D.B. SPALDING, A calculation procedure for heat, mass and momentum transfer in three-dimensional parabolic flows, *Int. J. Heat Mass Transfer*, **15**, pp. 1787-1806, 1972.

[7] L. DAVIDSON and P. HEDBERG, Mathematical derivation of a finite-volume formulation for laminar flow in complex geometries, *Int. J. Numer. Methods in Fluids*, **9**, pp. 531-540, 1989.

[8] W. RODI, Turbulence models and their applications in hydraulics, International Association of Hydraulics Research, Monograph, Delft, 1980.

[9] M.D. HUSSAIN, Mathematische Modellierung von turbulenten Auftriebsströmungen, PhD Thesis, University of Karlsruhe, Karlsruhe, 1980.

[10] M. LJUBOJA and W. RODI, Calculation of turbulent wall jets with an algebraic Reynolds stress model, *J. Fluids Engng.*, **102**, pp.350-356, 1980.

[11] M. LESCHZINER, An introduction and Guide to PASSABLE: A finite-volume-based code for two-dimensional boundary-layer flows, UMIST, Manchester, 1982.

[12] N.Z. INCE and B.E. LAUNDER, Computation of turbulent natural convection in closed rectangular cavities, Proc. 2nd U.K. Natn. Conf. on Heat Transfer, University of Strathclyde, Glasgow, Vol. 2, pp. 1389-1400, 1988.

[13] L. DAVIDSON, Second-order correction of the $k-\varepsilon$ model to account for non-isotropic effects due to buoyancy, *Int. J. Heat Mass Transfer*, **33**, No. 12, pp. 2599-2608, 1990.

[14] B.J. DALY and F.H. HARLOW, Transport equations of turbulence, Physics Fluids, **13**, pp. 2634-2649, 1970.

[15] K. HANJALIĆ and B.E. LAUNDER, Sensitizing the dissipation equation to irrotational strains, *J. Fluids Engng.*, 102, pp. 34-39, 1980.

[16] M.R. MALIN, Modelling the effects of lateral divergence on radially spreading turbulent jets, *Computers & Fluids*, **17**, No. 3, pp. 453-465, 1989.

[17] V. HAROUTUNIAN and B.E. LAUNDER, Second-moment modelling of free buoyant shear flows: a comparison of parabolic and elliptical solutions, In *Stably stratified flow and dense gas dispersion*, pp. 409-430, ed. by J.S. PUTTOCK, Claredon Press, Oxford, 1988.

[18] N.E. KOTSOVINOS and LIST, E.J., Turbulent buoyant jets. Part 1: Integral properties, *J. Fluid Mech.*, **81**, pp. 25-44, 1977.

[19] M.S. CHANDRASEKHARA, Study of vertical plane turbulent jets and plumes, PhD thesis, University of Iowa, Iowa, 1983.

[20] C.J. CHEN and W. RODI, Vertical turbulent jets: a review of experimental data, HMT, The Sience & Applications of Heat and Mass Transfer, Vol. 4, Pergamon Press, Oxford, 1980.